Impact of nuclear quantum effects on the structural inhomogeneity of liquid water

Berger, Arian ; Ciardi, Gustavo ; Sidler, David ; Hamm, Peter ; Shalit, Andrey

DOI: https://doi.org/10.1073/pnas.1818182116

The Impact of Nuclear Quantum Effects on the Structural Inhomogeneity of Liquid Water

Arian Berger[a,1], **Gustavo Ciardi**[a,1], **David Sidler**[a], **Peter Hamm**[a,2], **and Andrey Shalit**[a]

[a]Department of Chemistry, University of Zurich, Winterthurerstr. 190, CH-8057 Zürich, Switzerland

This manuscript was compiled on December 18, 2018

The 2D-Raman-THz response of liquid water is studied in dependence of temperature and isotope substitution (H_2O, D_2O and $H_2^{18}O$). In either case, a very short-lived (i.e., between 75-95 fs) echo is observed that reports on the inhomogeneity of the low-frequency intermolecular modes, and hence on the heterogeneity of the hydrogen-bond networks of water. The echo lifetime slows down by about 20% when cooling the liquid from room temperature to the freezing point. Furthermore, the echo lifetime of D_2O is $6.5 \pm 1\%$ slower than that of H_2O, and both can be mapped upon each other by introducing an effective temperature shift of $\Delta T = 4.5 \pm 1$ K. In contrast, the temperature dependent echo lifetimes of $H_2^{18}O$ and H_2O are the same within error. D_2O and $H_2^{18}O$ have identical masses, yet $H_2^{18}O$ is much closer to H_2O in terms of nuclear quantum effects. It is therefore concluded that the echo is a measure of the the structural inhomogeneity of liquid water induced by nuclear quantum effects.

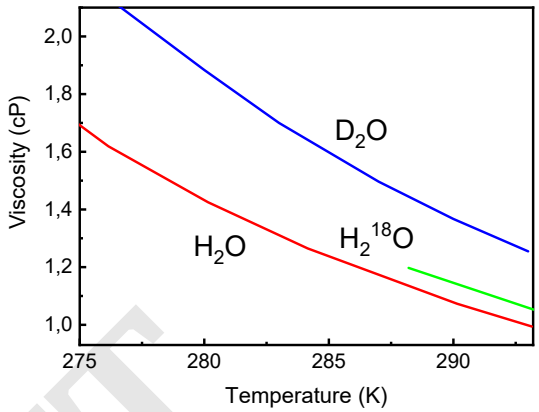

Fig. 1. Viscosity of H_2O (red), D_2O (blue) and $H_2^{18}O$ (green) in the temperature range relevant to this study. Data are compiled from Refs.(7, 15, 16)

The measurable variations in the different dynamical and thermodynamic properties of light (H_2O) and heavy (D_2O) water, which have been noted almost a century ago (1), are considered to be a clear manifestation of the quantum-mechanical nature of water (2). Due to the small mass of the proton, nuclear quantum effects (NQE) such as delocalization, zero point energy, and tunneling, modify the hydrogen bond strength/length and consequently the structure and dynamics of the hydrogen-bond networks, which in turn are considered to be the source of the anomalous behavior of water (3). The most prominent isotope effects include the elevation in the melting point and temperature of maximum density by 3.8 K and 7.2 K, respectively (4), and the increase in viscosity of about 23 % at room temperature upon deuteration of water (1, 5–7). The higher structural stability and slowdown in dynamics in D_2O are commonly explained by the stronger hydrogen bonds due to the reduced delocalization of the more classically behaving deuterium. For example, X-ray and neutron scattering confirmed that the oxygen-oxygen and oxygen-hydrogen radial distribution functions of D_2O are more structured than those of H_2O (8, 9). However, more elaborate models of competing quantum effect were put forward recently (10). That is, the anharmonicity of the OH-stretch potential renders the quantum-mechanical expectation value of the bond length longer in H_2O, thereby increasing the Coulombic interactions of the proton to a hydrogen-bonded water. This effect causes the lattice constant of H_2O ice Ih to be smaller than that of D_2O ice Ih (11, 12), and the question whether hydrogen bonding is stronger or weaker in H_2O does depend on the structure of the hydrogen bond networks (13). Also the inversion of the liquid-vapor isotope fractionation ratio at a certain temperature has been attributed to that effect (14).

The temperature-dependent viscosity is a particularly revealing observable to discuss isotope effects (Fig. 1). Robinson and coworkers (5) and later Harris and coworkers (6, 7) demonstrated that the temperature dependent viscosity η of D_2O (Fig. 1, blue) can be mapped onto that of H_2O (Fig. 1, red) by the following semi-empirical expression:

$$\eta_{D_2O}(T) = \sqrt{\frac{m_{D_2O}}{m_{H_2O}}} \cdot \eta_{H_2O}(T - \Delta T), \qquad [1]$$

where m is the mass of the two isotopologues. This mapping works remarkably well with an accuracy of 1% in a wide tem-

Significance Statement

The degree to which water is structured is an extremely intriguing problem and a matter of ongoing debates. To that end, we studied the 2D-Raman-THz response of liquid water in dependence of temperature and isotope substitution, considering H_2O, D_2O and $H_2^{18}O$. In either case, a very short-lived echo is observed, which is a measure of the inhomogeneity of the low-frequency intermolecular degrees of freedom of water. The echo decay time slows down with decreasing temperature, and differs for D_2O vs H_2O, while those of $H_2^{18}O$ and H_2O are the same. The comparison of the three isotopologues allows us to disentangle nuclear quantum effects from a trivial dynamical mass effect. It is found that the former are dominating the echo lifetime, and hence the heterogeneity of the hydrogen-bond networks of water.

A.B. and G.C conducted experiment and analyzed data, D.S. analyzed data, P.H. designed experiment and wrote the paper, A.S. conducted and designed experiment, analyzed data and wrote the paper.

[1]A.B. and G.C. contributed equally to this work.

[2]To whom correspondence should be addressed. E-mail: peter.hamm@chem.uzh.ch

perature range from T=243-323 K when assuming an effective temperature shift of ΔT=6.5 K. The physical reasoning for this expression is the following: if classical mechanics would apply, it can be shown on very general grounds that any thermodynamic property (e.g., melting point, density maximum, or the distribution of hydrogen bond networks as a function of temperature, etc.) would be the same for all isotopologues. This is since kinetic energy and potential energy partition functions separate, the latter of which being independent of nuclear mass (17). Dynamical properties (hydrogen-bond vibrational frequencies, self-diffusion or viscosity, etc.), on the other hand, scale with the square-root of mass (i.e., the first term in Eq. 1) both in classical and in quantum mechanics. Consequently, the second term in Eq. 1 accounts for NQEs. To that end, it is commonly assumed that H_2O at a given temperature is structurally very similar to D_2O at a somewhat elevated temperature, the idea being that enhanced thermal fluctuations in the latter case mimic zero-point fluctuations in the former case (10, 18–22). We stress though that the exact number of the temperature shift ΔT varies depending on observable (e.g., 3.8 K for the melting point vs 7.2 K for the density maximum), reflecting the fact that a temperature shift is of course only an effective (empirical) way to account for NQEs.

In this regard, the temperature dependent viscosity of $H_2^{18}O$, whose mass is the same as that of D_2O, is very instructive. It is only ∼5% larger than that of H_2O (Fig. 1, green) (16) and can be described as:

$$\eta_{H_2^{18}O}(T) = \sqrt{\frac{m_{H_2^{18}O}}{m_{H_2O}}} \cdot \eta_{H_2O}(T), \qquad [2]$$

i.e., with the mass factor but without any temperature shift. $H_2^{18}O$ exhibits the same NQEs as H_2O, since the major source of NQEs is the light proton in both cases. For example, the melting point and the density maximum of $H_2^{18}O$ differ by only 0.2-0.3 K from those of H_2O (4). Nevertheless, the mass factor does appear in Eq. 2 and accounts for the dynamical aspect of viscosity.

Conversely, Nilsson and coworkers have presented X-ray scattering results deep into the supercooled regime (23), and concluded that the D_2O data can be mapped onto the H_2O by applying the analogue of Eq. 1 with a temperature shift of ΔT=5 K, but without any mass factor. In light of the discussion above, that is expected, since scattering experiments measure essentially instantaneous snapshots of molecular structure, i.e., a purely thermodynamic aspect.

The hydrogen-bonding capability of water supports locally distinct structures that might live for a certain, relevant time span. If one were to instantaneously freeze all motion of liquid water, similar to amorphous ice, one would obtain structurally very heterogeneous snapshots, which would result in inhomogeneously broadened bands in all types of vibrational spectroscopies that are sensitive to molecular structure (e.g., dielectric relaxation and THz (24), IR (25–28), or Raman spectroscopy (29)). However, liquid water is of course very dynamic and those structures interconvert on very fast timescales, which has a tendency to render the spectroscopic response homogeneous. Being able to discriminate homogeneous from inhomogeneous broadening therefore will tell a lot about the amount of structuring in water and the lifetime of those structures.

However, conventional (1D) spectroscopic techniques cannot make the distinction between homogeneous and inhomogeneous broadening (30); that is the realm of photon echo and/or 2D spectroscopy (31). 2D IR spectroscopy has been applied widely to study the time-dependent inhomogeneity of the OH (or OD) stretch vibration of liquid water (32–36), revealing a typical lifetime of hydrogen bonds in the order of 1 ps. Furthermore, 2D THz-IR-VIS spectroscopy has been demonstrated recently that focuses on the coupling between inter- and intramolecular modes (37). However, the intramolecular OH stretch vibration is a high-frequency mode with $\hbar\omega \gg k_BT$, which is completely frozen at room temperature. A 2D spectroscopy fully in the THz regime would therefore be desired, where the intermolecular modes are found that are thermally excited and hence render liquid water a liquid.

Both 2D-Raman (38–43) as well as 2D-THz (44, 45) spectroscopy have been developed, but as of today, these experiments have not been feasible for liquid water. We (46, 47), as well as Blake and coworkers (48, 49), have therefore proposed 2D Raman-THz hybrid spectroscopies, which did result in the first 2D response of liquid water in the THz spectral range (50). We concentrate on the Raman-THz-THz pulse sequence with THz pulses peaking at ≈50 cm^{-1}, i.e., in the region of the hydrogen-bond bend vibration of liquid water, and spectrally extending into the hydrogen-bond stretch band at ≈200 cm^{-1}. In such an experiment, the Raman pump excites an intermolecular vibrational coherence, which after time t_1 is switched to another coherence state by a THz pump pulse. This coherence evolves as a function of time t_2 and emits a THz field that is detected. Among the many possible coherence pathways, there is a rephasing pathway that switches the sign of the coherence, which requires that the first Raman interaction induces a single-quantum transition, while the second THz interaction induces a two-quantum transition (51, 52). If the mode under consideration is inhomogeneously broadened on the time-scale of the pulse sequence, that coherence pathway will result in an echo, which peaks at a time t_2 that equals the time-separation t_1 between the two excitation pulses.

In pure water, we found that the signal is indeed slightly extended in the echo-direction $t_1 = t_2$ (50). Modelling the data base on a very simple model (a single anharmonic oscillator), we suggested that the echo originates mainly from the hydrogen-bond bend vibration at ≈200 cm^{-1}, and that a large fraction of its linewidth is attributed to quasi-inhomogeneous broadening in the slow-modulation limit with a correlation time of 370 fs (52). However, the echo is masked to a significant extent by the instrument response function, hence we set out in a subsequent publication (53) to artificially increase the amount of inhomogeneity by adding salts to the solution. This addition indeed extended the echo, and we found a strong correlation of the echo-decay time with the viscosity increase induced by a particular cation. For $MgCl_2$, which is characterized as a strong "structure maker" (54), the echo decay starts to exceed the free induction decay time along the t_1 axis, thereby establishing the concept of an echo in these experiments.

In the present paper, we explore how NQEs affect the lifetimes of structural inhomogeneities by directly comparing the extent of the echo signal of the 2D Raman-THz responses for H_2O and D_2O. We follow the temperature dependence and isotope shift of the echo lifetime from room temperature down

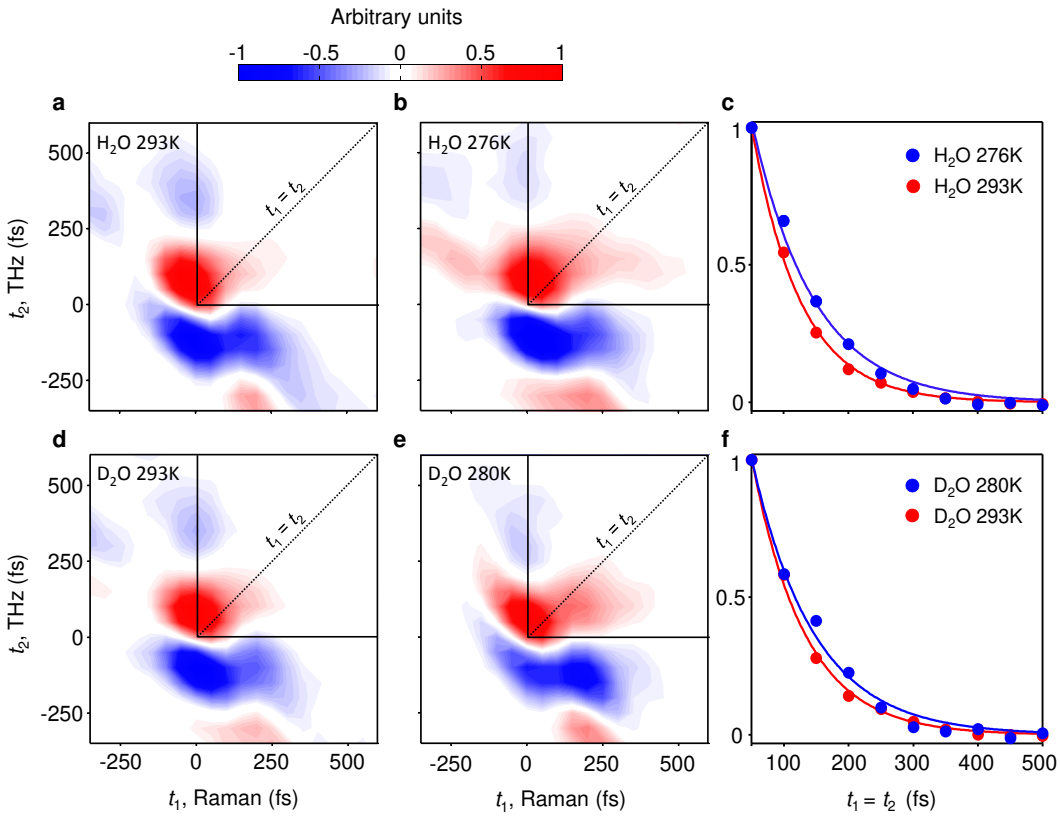

Fig. 2. 2D Raman–THz–THz responses of neat H_2O and D_2O at different temperatures. Full 2D signals for H_2O at (a) 293 K and at (b) 276 K, as well as for D_2O at (d) 293 K and at (e) 280 K. The upper-right quadrants, which correspond to the Raman–THz–THz pulse sequence, and the main diagonals $t_1 = t_2$ (dashed line) are indicated. Panel (c) compares 1D cuts along the $t_1 = t_2$ diagonal for H_2O at 293 K (dashed red line) and at 276 K (solid blue line), and panel (f) compares those for D_2O at 293 K (dashed red line) and at 280 K (solid blue line), in either case together with single-exponential fits (dashed lines). The 1D and 2D data are normalized to the maximum signal, and the 1D cuts start at 50 fs, after which time the effects of the pump-probe-pulse overlap can be neglected.

to their freezing points. We furthermore consider $H_2^{18}O$ in order to disentangle NQEs from trivial (classical) mass effects, in analogy to viscosity (Fig. 1). Along with a gradual increase in sample inhomogeneity with decreasing temperature for a given isotopologue, the observed isotope effects on the echo lifetime is attributed to NQEs.

1. Results

First, we measured the 2D Raman-THz signal of H_2O in a temperature range of 293 K-276 K. Fig. 2a,b serves to demonstrate the qualitative differences in the 2D response at the extreme temperatures considered in this study. As has been discussed previously (50, 52, 55), the measured signals in 2D Raman-THz spectroscopy are governed by the quite evolved instrument response function (IRF), which significantly smears out the real molecular signatures. We will focus our analysis on those parts of the 2D response that are less susceptible to such contaminations from the IRF , i.e., the diagonal t_1=t_2 in upper right quadrant (dotted lines in Fig. 2), along which an echo is expected in the Raman-THz-THz pulse sequence. Figs. 2a,b show that the relaxation dynamics along this diagonal becomes slower with decreasing temperatures. Fig. 2c presents 1D cuts along the diagonal together with single exponential fits (dashed lines), for which this trend is more clearly visible. Fig. 3 confirms that observation on a more quantitative level by plotting the relaxation times of H_2O (red) derived from the single exponential fits to the 1D cuts along t_1=t_2 against temperature. Overall, the decay can be modelled extremely well assuming a single-exponential function, and it slows down by almost 20% from 74±2 fs at room temperature to 95±2 fs at 276 K.

Next, we obtained the 2D Raman-THz responses for D_2O in the temperature range of 293-280 K. Figs. 2d,e show the full 2D signals observed at room temperature and close to the freezing point of D_2O, respectively, and Figs. 2f 1D cuts along the diagonal t_1=t_2. As in the case of H_2O, the signal along the diagonal is clearly extending with decreasing temperature. Fig. 3 reveals that the decay times for D_2O (blue) are consistently slower than for H_2O (red), ranging from 81±3 fs at room temperature to 98±2 fs at 280 K.

Analyzing the H_2O and D_2O results in the context of Eq. 1, we find that either one of the two correction factors could explain the difference in the echo decay time, but it turns out that both at the same time would overestimate the effect. That is, the difference in the echo decay time is 6.5 ± 1%; within signal-to-noise the same as the factor $\sqrt{m_{D_2O}/m_{H_2O}} = 1.054$. In that scenario, the difference in the echo decay time would reflect a (trivial) dynamical effect. Conversely, given the identical slope of the two plots, one may also shift the D_2O data onto the H_2O data by introducing an effective temperature shift of $\Delta T = 4.5 \pm 1$ K. Such a temperature shift is well within the range of what would be

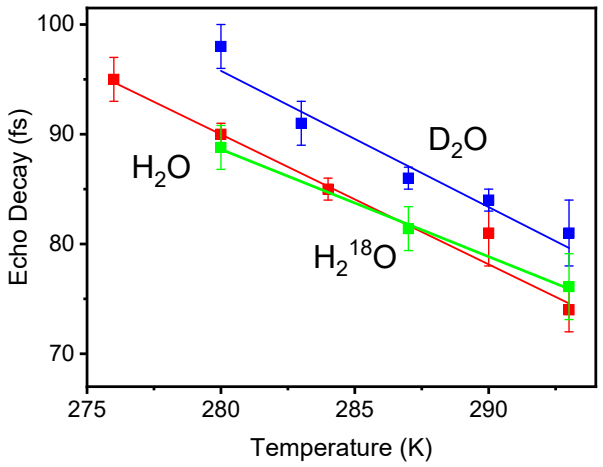

Fig. 3. Echo decay times of H_2O (red), D_2O (blue) and $H_2^{18}O$ (green) as a function of temperature. While H_2O and D_2O have been measured under absolutely comparable conditions and post-processed identically, $H_2^{18}O$ has been measured differently. For a direct comparison with the H_2O and D_2O data, the $H_2^{18}O$ data were up-scaled by 5%, as discussed in Materials and Methods. The lines are linear fits to guide the eyes.

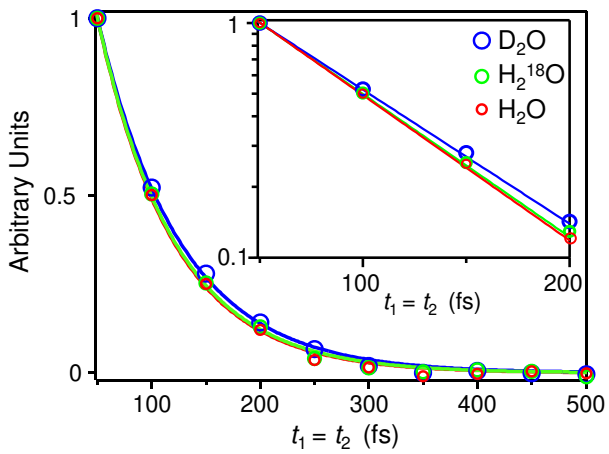

Fig. 4. 1D scan of the echo decay signal measured along the diagonal $t_1 = t_2$ for H_2O (red), D_2O (blue) and $H_2^{18}O$ (green) at 293 K, in either case together with single-exponential fits (dashed lines). The insert shows the same data on a log-scale. While these data have been measured slightly differently than those in Fig. 2 (see Materials and Methods for details), they are directly comparable among each other. The data are normalized to the maximum signal, and the cuts start at 50 fs, after which time the effects of the pump-probe-pulse overlap can be neglected.

considered a reasonable value for a NQE; e.g., it is about the same as the shift of the melting point (3.8 K). If that is the explanation for the difference, one would conclude that the echo lifetime measures the different degree of hydrogen bond structuring of H_2O vs D_2O.

From the results of H_2O and D_2O alone, we cannot decide which one of the two explanations is correct. We therefore now turn to $H_2^{18}O$, whose mass is the same as that of D_2O, which however equals H_2O in terms of NQEs. Fig. 4 compares the echo decay along the diagonal $t_1 = t_2$ for $H_2^{18}O$ (green) with those of H_2O (red) and D_2O (blue) at 293 K, all of which are measured under directly comparable conditions, and Fig. 3 (green) plots the echo decay time of $H_2^{18}O$ as a function of temperature. In either case, the result for $H_2^{18}O$ and H_2O are indistinguishable within error, while the echo decay of D_2O is clearly slower. This in turn evidences that the difference of H_2O vs D_2O is due to NQEs, and not due to a dynamical mass factor:

$$\tau_{D_2O}(T) = \tau_{H_2O}(T - \Delta T). \quad [3]$$

We therefore propose that the echo decay time indeed reflects NQEs.

2. Discussion and Conclusion

In light of the discussion of Eq. 1, it might seem puzzling that the square-root-mass factor is not observed in the echo decay time; after all, that is a dynamical aspect. We think of dephasing in a liquid like water in terms of "spectral diffusion", i.e. an ensemble of modes, whose frequencies fluctuate as a function of time with a characteristic correlation time τ_c (31):

$$\langle \delta\omega(t)\delta\omega(0)\rangle = \Delta\omega^2 e^{-t/\tau_c} \quad [4]$$

where $\delta\omega(t) = \omega(t) - \langle\omega(t)\rangle$ is the deviation from the mean of the transition frequency, and $\Delta\omega$ is the standard deviation of the frequency distribution. On the timescale τ_c, an instantaneously inhomogeneous ensemble converts into a homogeneous one. In the limes $\Delta\omega\tau_c \ll 1$, one would obtain purely homogenous dephasing with $T_2^* = (\Delta\omega^2\tau_c)^{-1}$, and in the limes $\Delta\omega\tau_c \gg 1$ statically inhomogenous broadening with an absorption band, whose width is $\Delta\omega$. In the inhomogenous limes, $\Delta\omega$ is the dominating factor determining the echo decay time, while the effect of τ_c is minor (which can be seen when calculating a rephasing coherence pathway in second order perturbation theory starting from Eq. 4, see Ref. (56)). While τ_c is a dynamical property, for which one would indeed expect to observe a square-root-mass factor, the distribution of frequencies is a purely thermodynamic property, which is mass-independent. Since we do not observe a difference in the echo decay time between H_2O vs $H_2^{18}O$, we conclude that we are in the inhomogenous limes, and indeed, a fit of the experimental data of H_2O at room temperature has revealed $\Delta\omega\tau_c \approx 5$ (i.e., τ_c=370 fs, $\Delta\omega$=75 cm^{-1}) (52).

Other aspects might however contribute as well to that issue. For example, any hydrogen-bond rearrangement requires the rotation of a water molecule (28, 57), which is governed by its moment of inertia and not its translational mass. The moment of inertia of $H_2^{18}O$, averaged over the three principal axes, is only 0.5% larger than that of H_2O, thereby providing another possible explanation for the mass-independence of the echo decay time. The D_2O results however speak against that scenario, since its moment of inertia is almost twice that of H_2O, yet the effect on the echo decay time is only 5%. Hence, hydrogen-bond switching events don't seem to be rate-determining for the echo-decay time. And indeed, the rotational diffusion times of H_2O and D_2O have been calculated using ring polymer molecular dynamics (RPMD) simulations, revealing a significantly larger difference of ∼30% at 298 K (28). About 1/3 of that effect has been attributed to the classical mass effect and the remainder to NQEs.

The discussion in the previous two paragraph emphasizes that our strict separation of Eq. 1 into a dynamical mass factor and NQEs is probably a bit of an oversimplification. In particular, both the effective mass (e.g., translational mass vs moment of inertia) and the effective temperature shift

needed to mimic NQEs depend on the degrees of freedom that are relevant for a given process. At the same time, the two correction factors cause similar shifts and are experimentally very difficult to disentangle, in particular when the considered temperature range is small. It appears that viscosity shown in Fig. 1 is a particularly straight-forward to interpret observable in this regard. We nevertheless think that our discussion of Eq. 1 is a valid starting point to set the stage, and that the comparison of H_2O vs D_2O vs $H_2^{18}O$ does contain the information needed to disentangle NQE from trivial (classical) mass effects.

A reasonable agreement of response calculations based on classical MD simulations with experimental 2D Raman-THz signals has been obtained when a proper force field is used (55). Combining these simulations with RPMD, thereby including NQEs, will be computationally very expensive, but is not out of reach. That is, while RPMD simulations of water have been connected to various spectroscopic observables, such as IR (26–28) or X-ray absorption spectroscopy (58), they required the calculation of only a two-timepoint correlation function, as they simulated one-dimensional responses. Converging a three-timepoint correlation function required for 2D-Raman-THz spectroscopy will be computationally much more expensive, but efficient concepts to perform this task have already be proposed (59). In any case, such simulations will be needed to test to what extent the very idea of Eq. 1 describes the 2D-Raman-THz echo of liquid water properly.

Materials and Methods

The experimental setup for 2D Raman THz spectroscopy has been introduced in detail in previous publications (50, 51, 53). In brief, a train of short (100 fs) 800 nm pulses with a bandwidth of 300 cm^{-1} (9 THz) delivered from a 5 kHz amplified Ti:sapphire laser system was split into three parts. The biggest fraction with energy of 200 μJ was used as Raman-pump, whose beam diameter in the sample has been 250 μm. The second beam with energy of 10 μJ was used to generate short THz pulses by means of optical rectification in a 100 μm thick (110) GaP crystal. Finally, the third weak portion of the fundamental beam (a few nJ's of energy) was used to detect the generated THz field in an identical GaP crystal by sensitivity-enhanced (60) electro-optic sampling and balanced detection. The pulse duration of the THz pulse was 140 fs, peaking at 1.4 THz and extending to 7 THz. The THz pulse was focused to 250 μm in the sample by means of a custom-made elliptical mirror with a numerical aperture close to 1. The delay between the Raman-pump and generated THz field, which define time t_1, was controlled with a conventional translational stage in steps of 50 fs, while the delay between THz generation and detection (time t_2) was controlled by a rapid scanning motor (APE), which allows for obtaining the entire THz wavefront in 1 s.

A 40 μm thick wire-guided gravity-driven water jet was used for the measurements (61) to avoid any signal contribution form a window material. The temperature of the water jet was controlled by an external water-ethanol bath, which cooled the water reservoir just above the jet. The temperature was measured in close proximity to the intersection region of Raman and THz pulses in the jet with an accuracy of $\pm$0.5 K.

Due to the small signal size, a substantial acquisition time is needed, typically on the order of 24 h per full 2D data set. The stability of the laser system and the water jet is a concern on that timescale. An active beam stabilization scheme was used to correct for beam walking of the laser system. To reduce drifts in the water jet thickness (e.g., due to evaporation of water), an active jet stabilization has been implemented, where the thickness of the jet was measured based on the time-delay of the transmitted THz pulse and was corrected by adjusting the water flow. Moreover, during the post-processing, the data, which consists of typically 300-500 individual 2D Raman-THz scans, were corrected for temporal drifts by adjusting the signal maxima in sequential data subsets with a typical size of 100 scans.

The diagonal signal shown in Fig. 2c,f were constructed by averaging over the main diagonal $t_1 = t_2$ and the first upper and lower off-diagonals, and their decay times were determined from single exponential fits. The major source of error in the decay time is the offset level for large times $t_1 = t_2$, which has been subtracted. To determine its uncertainty, the standard deviation of the background signal in the response-free quadrant ($t_1 < 0$ and $t_2 < 0$) has been estimated, from which the error in the decay time has been calculated. Great care was taken to measure H_2O and D_2O subsequently and under exactly the same conditions, and to post-process the data the same way, in order to be able to compare decay times with an accuracy of $\approx$1-2 fs.

To reduce the measurement time for the quite expensive $H_2^{18}O$, only the diagonal $t_1 = t_2$ has been measured, which results in a larger uncertainty of the time zeros $t_1 = t_2 = 0$, since one misses the peak of the 2D signal. Therefore, H_2O and D_2O have been measured as well along with $H_2^{18}O$ under exactly the same conditions. Fitting these H_2O and D_2O data revealed 5% faster time constants compared to those in Fig. 2. Consequently, the $H_2^{18}O$ data shown in Fig. 3 (green line) are up-scaled by that factor to facilitate a direct comparison.

ACKNOWLEDGMENTS. We thank Yoshitaka Tanimura for very valuable discussions. The work has been supported by the Swiss National Science Foundation (SNF) through the NCCR MUST.

1. Baker WN (1936) A New Comparison of the Viscosity of D2O with that of H2O. *Journal of Chemical Physics* 4(4):294–295.
2. Ceriotti M, et al. (2016) Nuclear Quantum Effects in Water and Aqueous Systems: Experiment, Theory, and Current Challenges. *Chemical Reviews* 116(13):7529–7550.
3. Debenedetti PG (2003) Supercooled and glassy water. *J. Phys.- Condens Matter* 15(45):R1669.
4. Steckel F, Szapiro S (1963) Physical properties of heavy oxygen water. *Transactions of the Faraday Society* 59:331–343.
5. Cho CH, Urquidi J, Singh S, Robinson GW (1999) Thermal Offset Viscosities of Liquid H 2 O, D 2 O, and T 2 O. *The Journal of Physical Chemistry B* 103(11):1991–1994.
6. Harris KR (2002) Isotope effects and the thermal offset effect for diffusion and viscosity coefficients of liquid water. *Physical Chemistry Chemical Physics* 4(23):5841–5845.
7. Harris KR, Woolf LA (2004) Temperature and volume dependence of the viscosity of water and heavy water at low temperatures. *Journal of Chemical and Engineering Data* 49(4):1064–1069.
8. Hart RT, et al. (2005) Temperature dependence of isotopic quantum effects in water. *Physical Review Letters* 94:047801.
9. Soper AK, Benmore CJ (2008) Quantum differences between heavy and light water. *Physical Review Letters* 101(6):065502.
10. Habershon S, Markland TE, Manolopoulos DE (2009) Competing quantum effects in the dynamics of a flexible water model. *Journal of Chemical Physics* 131(2):024501.
11. Röttger K, Endriss A, Ihringer J, Doyle S, Kuhs WF (1994) Lattice Constants and Thermal Expansion of H 2 0 and D 2 0 Ice Ih Between 10 and 265 K I . Introduction. *Acta Cryst.* B50:644–648.
12. Pamuk B, et al. (2012) Anomalous nuclear quantum effects in ice. *Physical Review Letters* 108(19):193003.
13. Pamuk B, Allen PB, Fernández-Serra MV (2018) Insights into the structure of liquid water from nuclear quantum effects on density and compressibility of ice polymorphs. *J. Phys. Chem. B* 122:5694–5706.
14. Markland TE, Berne BJ (2012) Unraveling quantum mechanical effects in water using isotopic fractionation. *Proc. Natl. Acad. Sci. USA* 109(21):7988–7991.
15. Dehaoui A, Issenmann B, Caupin F (2015) Viscosity of deeply supercooled water and its coupling to molecular diffusion. *Proceedings of the National Academy of Sciences* 112(39):12020–12025.
16. Kudish AI, Wolf D, Stecke F (1972) Physical Properties of Heavy-oxygen Water Absolute Viscosity of H218O between 15 and 35C. *J. Chem. Soc., Faraday Trans. 1* 172:2041–20462.
17. Chandler D (1987) *Introduction to Modern Statistical Mechanics.* (Oxford University Press, Oxford).
18. Kuharski RA, Rossky PJ (1985) A quantum mechanical study of structure in liquid H2O and D2O. *J. Chem. Phys.* 82:5164.
19. Stern HA, Rittner F, Berne BJ, Friesner RA (2001) No Title. *J. Chem. Phys.* 115:2237–2251.
20. Fanourgakis GS, Schenter GK, Xantheas SS (2006) A quantitative account of quantum effects in liquid water. *J. Chem. Phys.* 125:141102.
21. Paesani F, Iuchi S, Voth GA (2007) Quantum effects in liquid water from an ab initio-based polarizable force field. *Journal of Chemical Physics* 127(7):74506.
22. Hamm P, Fanourgakis GS, Xantheas SS (2017) A surprisingly simple correlation between the classical and quantum structural networks in liquid water. *The Journal of Chemical Physics* 147(6):064506.
23. Kim KH, et al. (2017) Temperature-Independent Nuclear Quantum Effects on the Structure of Water. *Physical Review Letters* 119(7):075502.

24. Ronne C, Astrand PO, Keiding S (1999) THz Spectroscopy of Liquid H2O and D2O. *Physical Review Letters* 82(14):2888–2891.
25. Bakker HJ, Rezus YLA, Timmer RLA (2008) Molecular Reorientation of Liquid Water Studied with Femtosecond Midinfrared Spectroscopy. *The Journal of Physical Chemistry A* 112(46):11523–11534.
26. Paesani F, Xantheas SS, Voth GA (2009) Infrared Spectroscopy and Hydrogen-Bond Dynamics of Liquid Water from Centroid Molecular Dynamics with an Ab Initio-Based Force Field. *J. Phys. Chem. B* 113:13118.
27. Paesani F, Yoo S, Bakker HJ, Xantheas SS (2010) Nuclear Quantum Effects in the Reorientation of Water. *Journal of Physical Chemistry Letters* 1(15):2316–2321.
28. Wilkins DM, Manolopoulos DE, Pipolo S, Laage D, Hynes JT (2017) Nuclear Quantum Effects in Water Reorientation and Hydrogen-Bond Dynamics. *Journal of Physical Chemistry Letters* 8(12):2602–2607.
29. Amo Y, Tominaga Y (2000) Low-frequency Raman study of water isotopes. *Physica A* 276(3-4):401–412.
30. Loring RF, Mukamel S (1985) Selectivity in coherent transient {R}aman measurements of vibrational dephasing in liquids. *J. Chem. Phys.* 83:2116–2128.
31. Hamm P, Zanni MT (2011) *Concepts and Methods of 2D Infrared Spectroscopy.* (Cambridge University Press, Cambridge).
32. Asbury JB, et al. (2004) Dynamics of water probed with vibrational echo correlation spectroscopy. *J. Chem. Phys.* 121:12431–12446.
33. Yeremenko S, Pshenichnikov MS, Wiersma DA (2003) Hydrogen-bond dynamics in water explored by heterodyne-detected photon echo. *Chem. Phys. Lett.* 369:107–113.
34. Cowan ML, et al. (2005) Ultrafast memory loss and energy redistribution in the hydrogen bond network of liquid H2O. *Nature* 434:199–202.
35. Eaves JD, et al. (2005) Hydrogen bonds in liquid water are broken only fleetingly. *Proc. Natl. Acad. Sci. USA* 102(37):13019–13022.
36. Perakis F, Widmer S, Hamm P (2011) Two-dimensional infrared spectroscopy of isotope-diluted ice Ih. *Journal of Chemical Physics* 134(20):1–9.
37. Grechko M, et al. (2018) Coupling between intra-and intermolecular motions in liquid water revealed by two-dimensional terahertz-infrared-visible spectroscopy. *Nature Communications* 9(1):885.
38. Tanimura Y, Mukamel S (1993) 2-Dimensional femtosecond vibrational spectroscopy of liquids. *J. Chem. Phys.* 99:9496–9511.
39. Blank DA, Kaufman LJ, Fleming GR (2000) Direct fifth-order electronically nonresonant {R}aman scattering from {CS$_2$} at room temperature. *J. Chem. Phys.* 113:771–778.
40. Kaufman LJ, Heo J, Ziegler LD, Fleming GR (2002) Heterodyne-Detected Fifth-Order Nonresonant Raman Scattering from Room Temperature <math display="inline"> <mrow> <msub> <mrow> <mi>CS</mi> </mrow> <mrow> <mn>2</mn> </mrow> </msub> </mrow> </math>. *Physical Review Letters* 88(20):207402.
41. Kubarych KJ, Milne CJ, Miller RJD (2003) Fifth-order two-dimensional {R}aman spectroscopy: a new direct probe of the liquid state. *Int. Rev. Phys. Chem.* 22(3):497–532.
42. Golonzka O, Demirdöven N, Khalil M, Tokmakoff A (2000) Separation of cascaded and direct fifth-order {R}aman signals using phase-sensitive intrinsic heterodyne detection. *J. Chem. Phys.* 113:9893–9896.
43. Li YL, Huang L, Miller RJD, Hasegawa T, Tanimura Y (2008) Two-Dimensional Fifth-order {R}aman spectroscopy of liquid formamide: Experiment and Theory. *J. Chem. Phys.* 128:234507.
44. Lu J, et al. (2016) Nonlinear two-dimensional terahertz photon echo and rotational spectroscopy in the gas phase. *Proc. Natl. Acad. Sci. USA* 113:11800–11805.
45. Woerner M, Kuehn W, Bowlan P, Reimann K, Elsaesser T (2013) Ultrafast two-dimensional terahertz spectroscopy of elementary excitations in solids. *New Journal of Physics* 15:025039.
46. Hamm P, Savolainen J (2012) 2D-Raman-THz Spectroscopy of Water: Theory. *J. Chem. Phys.* 136:94516.
47. Hamm P, Savolainen J, Ono J, Tanimura Y (2012) Note: Inverted time-ordering in two-dimensional-Raman-terahertz spectroscopy of water. *J. Chem. Phys.* 136:236101.
48. Finneran IA, Welsch R, Allodi MA, Miller TF, Blake GA (2016) Coherent two-dimensional terahertz-terahertz-Raman spectroscopy. *Proceedings of the National Academy of Sciences* 113(25):6857–6861.
49. Finneran IA, Welsch R, Allodi MA, Miller TF, Blake GA (2017) 2D THz-THz-Raman Photon-Echo Spectroscopy of Molecular Vibrations in Liquid Bromoform. *The Journal of Physical Chemistry Letters* 8:4640–4644.
50. Savolainen J, Ahmed S, Hamm P (2013) Two-Dimensional Raman-THz Spectroscopy of Water. *Proceedings of the National Academy of Sciences* 110(51):20402.
51. Hamm P, Shalit A (2017) Perspective: Echoes in 2D-Raman-THz Spectroscopy. *J. Chem. Phys.* 146:130901.
52. Sidler D, Hamm P (2018) Feynman diagram description of 2d-raman-thz spectroscopy applied to water. arXiv:1812.06742v1. Preprint, posted December 17, 2018.
53. Shalit A, Ahmed S, Savolainen J, Hamm P (2017) Terahertz echoes reveal the inhomogeneity of aqueous salt solutions. *Nature Chemistry* 9:273–278.
54. Jenkins HDB, Marcus Y (1995) Viscosity B-Coefficients of Ions in Solution. *Chem. Rev.* 95(8):2695–2724.
55. Hamm P (2014) 2D-Raman-THz spectroscopy: A sensitive test of polarizable water models. *Journal of Chemical Physics* 141(18):184201.
56. Steffen T, Duppen K (1998) Population relaxation and non-Markovian frequency fluctuations in third- and fifth-order Raman scattering. *Chemical Physics* 233(2-3):267–285.
57. Laage D, Hynes JT (2006) A Molecular Jump Mechanism of Water Reorientation. *Science* 311(5762):832–835.
58. Sun Z, et al. (2018) Electron-Hole Theory of the Effect of Quantum Nuclei on the X-Ray Absorption Spectra of Liquid Water. *Physical Review Letters* 121(13):137401.
59. Hasegawa T, Tanimura Y (2006) Calculating fifth-order Raman signals for various molecular liquids by equilibrium and nonequilibrium hybrid molecular dynamics simulation algorithms. *Journal of Chemical Physics* 125(7):1–7.
60. Ahmed S, Savolainen J, Hamm P (2014) Detectivity enhancement in {THz} electrooptical sampling. *Rev. Sci. Instrum.* 85:13114.
61. Tauber MJ, Mathies RA, Chen X, Bradforth SE (2003) Flowing liquid sample jet for resonance Raman and ultrafast optical spectroscopy. *Rev. Sci. Instrum.* 74:4958–4960.